Single-Cell RNA Analysis Reveals Cell-Intrinsic Functions of CAR T Cells Correlating with Response in a Phase II Study of Lymphoma Patients

Single-Cell RNA Analysis Reveals Cell-Intrinsic Functions of CAR T Cells Correlating with Response in a Phase II Study of Lymphoma Patients

Tina Sarén[1], Mohanraj Ramachandran[1], Gustav Gammelgård[1], Tanja Lövgren[1], Claudio Mirabello[2], Åsa K. Björklund[3], Kristina Wikström[4], Jamileh Hashemi[1], Eva Freyhult[5], Håkan Ahlström[6,7], Rose-Marie Amini[1], Hans Hagberg[1], Angelica Loskog[1,8], Gunilla Enblad[1], and Magnus Essand[1]

ABSTRACT

Purpose: Although CD19 chimeric antigen receptor T cells (CAR-T) therapy has shown remarkable success in B-cell malignancies, a substantial fraction of patients do not obtain a long-term clinical response. This could be influenced by the quality of the individual CAR-T infusion product. To shed some light on this, clinical outcome was correlated to characteristics of CAR-T infusion products.

Patients and Methods: In this phase II study, patients with B-cell lymphoma ($n = 23$) or leukemia ($n = 1$) received one or two infusions of third-generation CD19-directed CAR-Ts ($2 \times 10^8/m^2$). The clinical trial was registered at clinicaltrials.gov: NCT03068416. We investigated the transcriptional profile of individual CD19 CAR-T infusion products using targeted single-cell RNA sequencing and multicolor flow cytometry.

Results: Two CAR-T infusions were not better than one in the settings used in this study. As for the CAR-T infusion products, we found that effector-like $CD8^+$CAR-Ts with a high polyfunctionality, high cytotoxic and cytokine production profile, and low dysfunctional signature were associated with clinical response. An extended *ex vivo* expansion time during CAR-T manufacturing negatively influenced the proportion of effector $CD8^+$CAR-Ts in the infusion product.

Conclusions: We identified cell-intrinsic characteristics of effector $CD8^+$CAR-Ts correlating with response that could be used as an indicator for clinical outcome. The results in the study also serve as a guide to CAR-T manufacturing practices.

Introduction

Remarkable results have been achieved using CD19-targeting chimeric antigen receptor T cells (CAR-T) against B-cell malignancies (1–7). However, there are still patients that do not respond, so in order to achieve sustained complete responses (CR), several hurdles need to be overcome. These include manufacturing failure, primary resistance to treatment, and relapse after initial response (8). The contribution of each of these factors to long-term response varies across different B-cell malignancies. In early studies, the primary response rates were slightly higher in patients with B-cell acute lymphoblastic leukemia (ALL) compared with patients with large B-cell lymphoma (LBCL) and especially compared with patients with chronic lymphocytic leukemia (8). Although the primary response rates are now comparable in patients with LBCL and ALL (6, 7, 9) relapses are less frequent in LBCL in comparison with ALL. To further improve the response for patients, factors contributing to primary resistance to CAR-T treatment must be addressed (8).

Parameters that have consistently been associated with response to CAR-T therapy across different studies include disease histology and the lymphodepleting preconditioning used (8). Other factors correlating with response are disease dependent, for example, high CAR-T expansion in patient blood is associated with response in ALL (10, 11). However, the contribution of CAR-T *in vivo* expansion to response in LBCL is contradictory (2, 12). The characteristics of the CAR-T infusion product can influence the response to CD19 CAR-T treatment in patients with LBCL (13). The status of the starting material for CAR-T production (harvested patients' T cells) can also influence treatment response (14, 15). These studies highlight the importance of further investigating preclinical parameters in all steps of the manufacturing process to find potential markers correlating with response. Such markers could, apart from predicting response, also suggest modifications to the manufacturing process to improve the CAR-T products.

We have previously evaluated the efficacy and safety of a third-generation CD19-targeting CAR-T construct, with CD3ζ, CD28, and 4–1BB intracellular signaling domains, in patients with advanced B-cell lymphoproliferative disease (16). In this study, we evaluated the feasibility and efficacy of administering two doses of these third-generation CAR-Ts. We also performed a detailed characterization of the individual CAR-T infusion products using single-cell RNA sequencing (scRNA-seq) and multicolor flow cytometry, and identified that an effector-like $CD8^+$CAR-T subpopulation with a cytokine and cytotoxic signature is associated with clinical response.

[1]Department of Immunology, Genetics and Pathology, Uppsala University, Science for Life Laboratory, Uppsala, Sweden. [2]IFM Bioinformatics, National Bioinformatics Infrastructure Sweden, Science for Life Laboratory, Linköping University, Linköping, Sweden. [3]Department of Life Sciences, National Bioinformatics Infrastructure Sweden, Science for Life Laboratory, Chalmers University of Technology, Göteborg, Sweden. [4]VECURA, Karolinska University Hospital Huddinge, Stockholm, Sweden. [5]Department of Medical Sciences, Uppsala University, Uppsala, Sweden. [6]Department of Surgical Sciences, Uppsala University, Uppsala, Sweden. [7]Antaros Medical AB, Mölndal, Sweden. [8]Lokon Pharma AB, Uppsala, Sweden.

T. Sarén and M. Ramachandran contributed equally as first authors of this article.

G. Enblad and M. Essand contributed equally as co-senior authors of this article.

Corresponding Author: Tina Sarén, Uppsala University, Department of Immunology, Genetics and Pathology, Uppsala, 751 85, Sweden. E-mail: tina.saren@igp.uu.se

Clin Cancer Res 2023;29:4139–52

doi: 10.1158/1078-0432.CCR-23-0178

Translational Relevance

Our study highlights the importance of performing detailed, single-cell characterization of chimeric antigen receptor T-cell (CAR-T) products as it identified a T-cell subset correlating with response. Identified T-cell subsets correlating with response could be used as an indicator for clinical outcome in future studies. It further highlights the importance of the CAR-T manufacturing process and suggests that maintaining a shorter *ex vivo* expansion time generates more functional CAR-T cells. Therefore, our study serves as a useful guide to manufacturing practices.

Patients and Methods

Clinical trial design

The clinical trial (EudraCT 2016–004043–36; NCT03068416) was a phase II, open-label, one-armed, single center trial. The clinical objectives were to evaluate safety and feasibility of two administrations of third-generation CD19-directed CAR-Ts to patients with disseminated B-cell lymphoma or leukemia, to evaluate long-term toxicity of CAR-T, and to evaluate whether two courses of gemcitabine given in association with the second dose of CAR-Ts can increase the effect of CAR-T therapy. All patients were treated at the Uppsala University Hospital (Uppsala, Sweden). The trial was approved by the Swedish Medical Product Agency (5.1–2017–6020 with amendment 5.1–2019–12385) and by the regional Ethical Review Board (Dnr 2017/053 with amendment 2019–02326), and conducted in accordance with the Declaration of Helsinki. All patients had relapsed or refractory $CD19^+$ B-cell lymphoma or leukemia with no other curative treatment option available and measurable disease. Written informed consent was obtained from all patients. Study representation is shown in Supplementary Table S1.

After enrollment, 50 mL of peripheral blood was extracted for CAR-T production. Bridging chemo- or radiotherapy was used during the manufacture of CAR-Ts to control disease and reduce tumor burden. Lymphodepleting therapy was given with fludarabine 25 mg/m^2 daily on days −4 to −2 and cyclophosphamide 500 mg/m^2 on day −4. At day −1, patients with lymphoma were examined with FDG-PET MRI. A total of 2×10^8/m^2 CAR-Ts were administered through intravenous infusion on day 0. Patients were then followed weekly with blood biochemistry, blood counts, and clinical visits.

A second dose of CAR-T was administered if patients did not develop a cytokine release syndrome (CRS) or neurological toxicity of a grade ≥3. The second dose was followed by 2 courses of chemotherapy with gemcitabine 800 mg/m^2 after the second dose, attempting to control myeloid-suppressor cells (17). The second dose was not given to patients with severe cytopenia or rapid clinical progression and deterioration.

The response was evaluated at 1 month with FDG-PET-MRI when available ($n = 20$), otherwise with FDG-PET-CT ($n = 3$). The Lugano classification for response assessment of lymphomas was used (18). One patient with ALL was evaluated with bone marrow (BM) examination. In a few patients, a second FDG-PET-MRI was performed later but, in most patients, subsequent radiology was FDG-PET-CT or CT. Patients with ALL were evaluated with BM investigation.

CAR-T production

The CAR-Ts were manufactured by the Vecura GMP facility at the Karolinska University Hospital (Huddinge, Sweden), as previously described (16). In brief, peripheral blood mononuclear cells (PBMC) were prepared from 50 mL autologous peripheral heparinized blood by Ficoll (GE Healthcare) density gradient centrifugation. The fresh (non-cryopreserved) PBMCs were cultured in RPMI and Eagle's Hank's Amino Acids culture media (1:1 ratio) supplemented with 10% FCS and 2 mmol/L L-glutamine, in culture plates/flasks coated with anti-CD3 (1 μg/mL, OKT3, Miltenyi Biotec) and anti-CD28 (1 μg/mL, Miltenyi Biotec) for 2–3 days. From day 2, IL2 (200 IU/mL, Miltenyi Biotec) was added. Cells were transduced with a GMP-grade retroviral vector (Moloney murine leukemia virus), produced at the Center for Cell and Gene Therapy at Baylor College of Medicine (Houston, TX), encoding for CAR SFG αCD19.28.4–1BB-ζ (19) in retronectin (TaKaRa/Clonetech)-coated plates. Transduced cells were cultured under continuous IL2 supplementation until the target T-cell number was reached and were then frozen in therapeutic doses. The product was released after quality control (QC; enough cells for dose, no bacterial contamination, <5.0 EU/kg endotoxin, negative for *Mycoplasma*, >10% transgene expression, and no detectable autonomous growth) and transported on dry ice to Uppsala University Hospital (Uppsala, Sweden).

CAR-T detection in blood by quantitative PCR

Genomic DNA was prepared from 200 μL whole blood using the QIAamp DNA Blood Mini Kit (Qiagen) according to the manufacturer's protocol. Concentration was measured using the Qubit dsDNA BR assay kit (Thermo Fisher Scientific) using Qubit 3.0 fluorometer (Thermo Fisher Scientific). Quantitative PCR was carried out using 50 ng of genomic DNA as template. Reactions were performed with TaqMan Fast Advanced Master Mix (Thermo Fisher Scientific) with custom-made CAR-specific primers and probe (fwd: TGCCGATTTC-CAGAAGAAGAAGAAG, rev: TGCGCTCCTGCTGAACT, probe: FAM-CACTCTCAGTTCACATCCT-NFQ/MGB; Custom plus TaqMan RNA Assay, Thermo Fisher Scientific). Reactions were run on a Bio-Rad CFX96 Touch real-time PCR detection system (Bio-Rad).

Single-cell library preparation for targeted transcriptome sequencing and protein analysis

Targeted RNA and protein single-cell libraries were obtained using the BD Rhapsody platform (BD Biosciences). Patient-derived CAR-Ts were thawed and stained with the Zombie Aqua Fixable Viability Kit (#423101, BioLegend) and Fc block (#564220, BD Biosciences) according to the manufacturer's protocol. Cells were subsequently labeled with sample tags from the BD Human Immune Single-Cell Multiplexing Kit (#633781, BD Biosciences) and BD Ab-seq Ab-Oligos (Supplementary Table S2). Live cells were enriched for by sorting in BD FACSAria III Cell Sorter (BD Biosciences). After sorting, viability was measured in the BD Rhapsody analysis system and subsequently CAR-Ts from 6 patients were pooled at an equal ratio to obtain approximately 20,000 cells in total and added up to 620 μL with ice-cold Sample Buffer (#650000062, BD Biosciences). The pooled cells were then loaded in a BD Rhapsody cartridge (#633733, BD Biosciences) and mRNA captured with Cell Capture Beads (#650000089, BD Biosciences) according to the manufacturer's protocol. Captured mRNA was used as template to synthesize cDNA with the BD Rhapsody cDNA kit (#633773, BD Biosciences) according to the manufacturer's protocol. Subsequently, targeted libraries of genes in the human BD Rhapsody immune response panel Hs (# 633750, BD Bioscience), together with some additionally selected genes (Supplementary Table S3), Abseq Ab-Oligos and sample tags were prepared using BD Rhapsody Targeted mRNA and Abseq Amplification Kit (#633774, BD Biosciences). Concentration of the sequencing library was assessed using the Qubit dsDNA HS Kit (#Q32854, Thermo Fisher

Scientific) and fragment size was measured using the Agilent 2200 TapeStation with HS D5000 ScreenTape (#5067–5592, Agilent Technologies). In total, four separate targeted libraries were produced with 6 patients per library. The mRNA, Abseq, and Sample-tag amplicons from the four different libraries were diluted to 2 nmol/L and pooled for paired-end (Read1: 64bp, Read2: 55bp + i7 Indexes: 8bp) sequencing on NovaSeq 6000 S1 sequencer (Illumina) at the SNP&SEQ Technology Platform (Uppsala, Sweden).

Analysis of scRNA-seq data

QC

The raw scRNA-seq data were pre-processed by BD Biosciences using the Rhapsody Analysis pipeline (20) to convert the raw reads into Unique Molecular Identifier (UMI) counts. UMIs were further adjusted within Rhapsody by applying BD's Recursive Substitution Error Correction and Distribution-based Error Correction to remove false UMIs caused by sequencing or library preparation errors. Pooled samples were deconvoluted using Sample-tag reads. A cell was annotated as a singlet if the minimum read count for a given Sample-tag was attained and if more than 75% of the Sample-tag reads were derived from a single Sample-tag antibody. Multiplets were assigned if the count for two or more Sample-tag antibodies exceeded the minimum threshold. Cells were assigned as undetermined if they did not reach the criteria for either a singlet or multiplet. Whenever a cell was labeled as a multiplet or as undetermined, it was filtered out in the subsequent steps of the analysis. The final read depths for the libraries were in the following range: mRNA 8,888 to 13,006 average reads/cell and 94%–95% sequencing saturation, and AbSeq 1,995 to 4,672 average reads/cell and 39%–46% sequencing saturation, which were in the expected range of the manufacturer's recommendations for targeted transcriptomics sequencing (BD Biosciences)

The scRNA-seq and AbSeq counts were loaded and processed with Seurat v. 4.0.0 (21). Counts for the *CAR* gene were excluded from the scRNA-seq count matrices and kept as a separate metadata field to avoid introducing biases when clustering CAR^+ and CAR^- cells. Low-quality cells were filtered by sorting the cells from the highest to the lowest read count separately for each library. The cumulative count curve was then plotted for each library, and a cutoff point was defined at the first inflection point of the curve for each library. All cells above such cutoff point were labeled as low quality and excluded from subsequent analyses.

Clustering and differential gene expression

The scRNA-seq counts were log-normalized with scale factor of 10,000 and rescaled to regress out the number of detected genes per cell as a confounding factor. Detection of highly variable genes showed that all genes for which expression was not null for all cells were considered variable. Dimensionality reduction was first performed with principal component (PC) analysis with 30 components. A subset of 20 PCs was then manually selected from the elbow plot of the standard deviation of each PC, and used to perform non-linear dimensionality reduction with uniform manifold approximation and projection (UMAP; arXiv:1802.03426). The 2D UMAP embedding was used for all subsequent visualization purposes. The top 20 PCs were used to build a graph of neighboring cells using Seurat's *k*-nearest neighbors (22) function with $k = 20$. Clustering was then performed on the neighbor's graph using Seurat's shared nearest neighbor function at resolution 0.6. Each of the resulting clusters was then classified as a CD4 or CD8 cluster based on the mean expression of *CD4* and *CD8A* genes, respectively, and saved as Seurat objects for clustering fine-tuning and differential gene expression.

The Seurat objects were imported into Partek Flow build version 10.0.21.0411 (Partek Inc.) for subsequent downstream analysis. Biomarkers for each cluster and differentially expressed genes (DEG) between responders and non-responders were computed using the ANOVA test with Benjamini–Hochberg tests to correct for the false discovery rate (FDR) value of ≤0.05. Biomarkers for CD8 and CD4 clusters can be found in Supplementary Table S4. For correlation analysis, we calculated Pearson's coefficient with Benjamini–Hochberg tests to correct for FDR (Supplementary Table S5). The AUCell tool (23) in Partek Flow was used to identify cells that highly expressed genes belonging to well-described T-cell states (Supplementary Table S6). More detailed statistical analyses are mentioned in the respective figure legends.

GO term analysis

To test for enriched Gene Ontology (GO) Biological Processes, the DEGs from responder's versus non-responders (Supplementary Table S7) were uploaded to the online gProfiler tool (https://biit.cs.ut.ee/gplink/l/uNqpTde1Si). GO processes that were significantly enriched either in responders or non-responders are shown in **Fig. 3C**.

Detection and analysis of polyfunctional cells

The scRNA-seq counts were used to detect whether a cell could be included in one of several polyfunctional classes (Regulatory, Effector, Stimulatory, Chemoattractive, Inflammatory, and Inhibitory). Each class is determined by a list of genes associated to it according to the literature. A cell was assigned to a class whenever the expression of at least one gene in the corresponding list was higher than the median of non-zero counts for that given gene across the dataset. Whenever a cell was assigned to more than one polyfunctional class, the cell was classified as polyfunctional, and the fraction of polyfunctional cells was calculated for each patient.

We have developed the single-cell Polyfunctional Strength Index (scPSI) by adapting the PSI (24) of single-cell data. This was calculated for each patient sample *s* following the formula:

$$scPSI_s = \frac{\sum_{g=1}^{G} \sum_{pc=1}^{PC} counts_{g,pc}}{G \cdot C}$$

where the raw gene counts are summed up for each polyfunctional gene *g* and polyfunctional cell *pc* for that given sample and normalized by the total number of polyfunctional genes *G* multiplied by the total number of cells (polyfunctional or not) *C* in the sample.

To compare polyfunctionality across response classes (responders, non-responders), we performed bootstrapping by randomly selecting 50 cells for each patient and calculating the cumulative scPSI score for each response class. The bootstrap procedure was performed 1,000 times and used to estimate the mean for the scPSI scores in each response while avoiding biases from patients with larger amounts of polyfunctional cells. The difference between responses is tested by computing the fraction of tests (out of 1,000) that agree with the null hypothesis, that is, whenever the mean scPSI for a subset of cells from non-responders is higher than the mean scPSI for an equally sized subset of cells from responders. This fraction is then doubled to obtain the two-sided test *P* value.

Proteomics analysis of plasma

Plasma was collected from heparin tubes before CAR-T infusion (preCAR) and at follow-up post-treatment. Samples were stored at −80°C until analysis. The preCAR, 1 week (w) and 3 weeks post-treatment samples were analyzed for all treated patients except patient 5 ($n = 23$). In addition, samples 3 months post-treatment and pre- and post-gemcitabine were analyzed when applicable. Plasma samples were analyzed using the Inflammation panel (#95302, Olink).

Protein level association with side effect is analyzed using mixed effects linear regression (function lmer in the R-package lme4 (25), with normalized protein expression (NPX) as dependent variable and CRS (2–3 vs. 0–1) as well as age, sex, time point (preCAR, 1w or 3w), and the interaction between CRS and time point as fixed effects independent variables and patient ID as random effects variable. Results can be found in Supplementary Tables S8–S10.

The association between var and NPX at each of the time points separately is computed in *post hoc* contrast tests. All *post hoc* tests were performed using estimated marginal means implemented in the R-package emmeans (26).

The proteins are studied one at the time and the resulting P values will be adjusted for multiple tests (adjusting for the number of investigated proteins) using the Benjamini–Hochberg's method for controlling the FDR. The adjusted P value is reported in tables as q and associations are deemed significant if $q < 0.05$.

Cell lines and primary cell culture conditions

The human B lymphoma cell line Daudi (ATCC, CCL-213) was cultured in RPMI-1640 supplemented with 10% FBS, 1% penicillin/streptomycin (PEST), and 1% sodium pyruvate. Cells were tested for *Mycoplasma* before the experiments were performed to ensure negativity. The cells were not authenticated. Cells were used for experiments within 2 weeks after thawing. Upon thawing, the CAR-T patient batches were maintained in culture medium (RPMI-1640) supplemented with 10% FBS, 1% PEST, 1% sodium pyruvate, and IL2 (50 IU/mL, Proleukin, Novartis). All reagents were purchased from Thermo Fisher Scientific, unless mentioned otherwise.

Flow cytometry

CAR-T batch analysis

Patient-derived CAR-T batches were thawed and either analyzed immediately or rested overnight in culture medium with 50 IU/mL IL2. CAR-Ts were co-cultured together with target cells (Daudi) at a 1:1 effector to target ratio overnight before analysis and the co-culture supernatant was collected for ELISA. For analysis, unstimulated and stimulated CAR-Ts were first washed with FACS Buffer (PBS with 3 mmol/L EDTA and 0.1% BSA) and then re-suspended in Fixable Viability Stain (#565388, BD Biosciences). After washing, cells were re-suspended in Fc-block (# 564219, BD Biosciences) according to the manufacturer's protocol. After blocking, cells were washed twice with FACS Buffer before staining surface markers with antibodies that were conjugated with fluorochromes (Supplementary Table S11) in Brilliant Stain Buffer (#563794, BD Biosciences). Samples were run in CytoFLEX LX (Beckman Coulter) and analyzed using FlowJo (FlowJo LLC).

CAR-T batch functionality analysis

Patient-derived CAR-T batches were thawed and rested overnight in culture medium with 25 IU/mL IL2. CAR-Ts were either left untreated or were co-cultured together with target cells (Daudi) at a 1:1 effector to target ratio for 6 hours in presence of Protein Transport Inhibitor (#555029, BD Biosciences) before analysis. For analysis, T cells were washed with FACS Buffer (PBS with 3 mmol/L EDTA) and re-suspended in Fixable Viability Stain (#565388, BD Biosciences) containing Fc-block (#564219, BD Biosciences) according to the manufacturer's protocol. After blocking, cells were washed twice with FACS Buffer containing 0.1% BSA before staining surface markers with antibodies that were conjugated with fluorochromes (Supplementary Table S12) in Brilliant Stain Buffer (#563794, BD Biosciences). After staining, cells were washed and subsequently fixed and permeabilized using Cytofix–Cytoperm (#554714, BD Biosciences) according to the manufacturer's protocol. Intracellular markers were stained with fluorochrome conjugated antibodies (Supplementary Table S12) in Perm/Wash Buffer (#554714, BD Biosciences). After staining, cells were washed twice with Perm/Wash Buffer and subsequently fixed with 1% paraformaldehyde before analysis the same or following day. Samples were run in CytoFLEX LX (Beckman Coulter) and analyzed using FlowJo (FlowJo LLC)

Cytokine detection in co-culture supernatant

The supernatants from overnight co-culture of CD19-positive target cells (Daudi) and patient-derived CAR-Ts from the flow cytometry analysis (explained above) were used for detection of IFNγ by ELISA. The co-culture supernatants from experimental duplicates were pooled. Before ELISA, the supernatant was diluted 1:4 and ELISA was performed in experimental duplicates according to the manufacturer's protocol (Mabtech AB).

Statistical analysis

Information about statistical analysis can be found in each figure legend.

Data and code availability

Sequencing data generated during the current study are not publicly available due to the European General Data Protection Regulation to protect patients' privacy but are available from the corresponding author on reasonable request (DOI: 10.17044/scilifelab.20208764; https://figshare.scilifelab.se/articles/dataset/Targeted_scRNA-seq_and_AbSeq_of_human_CAR-T_cell_infusion_product_from_24_cancer_patients/20208764). Processed RNA-seq and AbSeq count files, raw and normalized, are available upon request on BioStudies (Accession: E-MTAB-12407; https://www.ebi.ac.uk/biostudies/arrayexpress/studies/E-MTAB-12407). R code used to process the data is available on the study GitHub repository: https://github.com/magnessa/EudraCT_2016-004043-36.

Results

Patients, CAR-T treatment, clinical response, and toxicity

The study included 28 patients of which 24 patients received CAR-T treatment (**Fig. 1A**). Treated patients had diffuse LBCL (DLBCL; $n = 21$), indolent B-cell lymphoma ($n = 2$; one follicular and one marginal zone lymphoma), or ALL ($n = 1$; **Fig. 1B**). Individual patient characteristics before CAR-T treatment are displayed in **Fig. 1B**. Patients received either one ($n = 10$) or two CAR-T doses ($n = 14$; **Fig. 1A**), with preconditioning only given at the first dose. A second CAR-T dose was not given to 10 patients due to CAR-T–related adverse events, including cytopenia ($n = 4$), CRS grade 3 ($n = 2$), clinical deterioration ($n = 3$), or limited amount of CAR-T ($n = 1$). Four patients were not treated due to CAR-T production failure ($n = 1$), or rapid clinical deterioration ($n = 3$). A detailed description of the patients, clinical procedures, response rate, and related toxicities is presented in Supplementary Tables S13 and S14.

The overall response rate (ORR), that is, CR and partial response at 1 month after the first CAR-T infusion was 38% (9/24; **Fig. 1C**) and the best ORR was 50% (12/24). The median progression-free survival (PFS) was 105 days (21–1,373+ days) and the median overall survival (OS) was 316 days (57–1,413+ days; **Fig. 1D** and **E**). OS correlated with PFS (**Fig. 1F**). A univariate cox regression analysis of lymphoma patient characteristics and clinical procedures revealed that only C-reactive protein (CRP) level and metabolic tumor volume (MTV) before CAR-T infusion could impact OS and PFS (Supplementary Table S15). An association between MTV and survival has previously

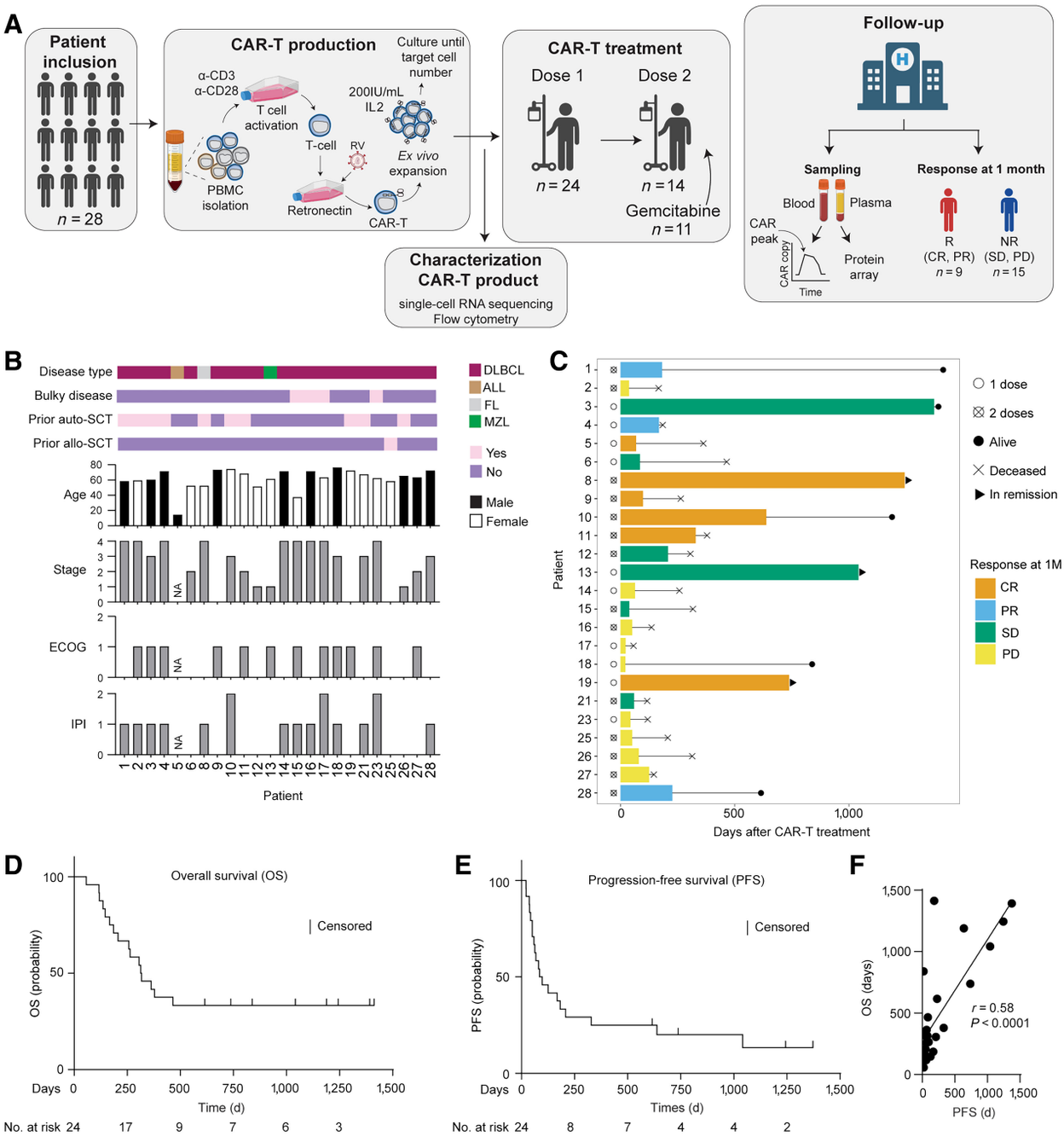

Figure 1.

A schematic overview of the patient cohort, trial design, and clinical outcome. **A,** Schematic illustration of the clinical trial from patient inclusion, CAR-T manufacturing, and treatment to follow-up. Patients were divided into responders (R), including complete response (CR) and partial response (PR), and non-responders (NR), including stable disease (SD) and progressive disease (PD) based on the response to CAR-T therapy at 1 month after treatment. Response was determined using FDG-PET-MRI ($n = 20$) or FDG-PET-CT ($n = 3$). **B,** Summary of patient characteristics before CAR-T infusion. ECOG, Eastern Cooperative Oncology Group performance status scale; IPI, International Prognostic Indices in diffuse large B-cell lymphoma. **C,** Swimmer plot of patient outcomes and number of CAR-T infusions (white circle, one; crossed circle, two). Bars represent progression-free survival and are colored according to response to CAR-T therapy at the one-month follow-up (orange, CR; blue, PR; green, SD; and yellow, PD). Line represents survival until deceased (cross) or last follow-up (black circle). Arrows at the end of a bar represent ongoing response. Kaplan–Meier estimates of (**D**) overall survival (OS) and (**E**) progression-free survival (PFS) in patients who received CAR-T therapy. **F,** Correlation between OS and PFS. Each dot represents data from one patient. Correlation analysis was performed using Pearson correlation. (**A,** Created with BioRender.com.)

been reported in a separate publication of the current clinical trial (27), but not in relation to the same factors as used in this study. Both MTV and CRP were still related to OS, but only MTV was related to PFS in a multivariate analysis (Supplementary Table S15). CRP was further able to separate patients with lymphoma into two groups using both OS ($P = 0.02$) and PFS ($P = 0.047$) as outcome (Supplementary Fig. S1A and S1B). Two courses of gemcitabine were given to 11 patients in association with the second CAR-T infusion (**Fig. 1A**) to improve the effect of CAR-T therapy by reducing myeloid-derived suppressor cells (17). However, no improvement of OS or PFS was observed in patients receiving gemcitabine (Supplementary Table S15). Of note, the two patients with indolent lymphoma (one follicular and one marginal zone lymphoma) are remaining in CR without further treatment 1,042+ and 1,244+ days. The patients who received two doses of CAR-Ts did not have a better PFS or OS compared with the patients who received one dose of CAR-T (Supplementary Fig. S2A and S2B; Supplementary Table S15). The CAR-T level in blood typically reached the peak within one to three weeks after the first infusion (Supplementary Fig. S2C–S2F). However, only 4 (patients 9, 10, 12, 16) out of the 14 patients who got two doses had an increase of CAR-Ts in their blood after the second infusion (Supplementary Fig. S2F). As receiving a second dose of CAR-T did not have a significant impact on PFS or OS, patients receiving one and two doses were from then on evaluated together. Patients were divided into responders (R, $n = 9$; overall/objective response) if they showed a radiological response at the one month follow-up and as non-responders ($n = 15$) if no radiological response was observed (**Fig. 1A**). Responding patients had a significantly better OS and PFS compared with non-responders (Supplementary Fig. S3A and S3B).

The toxicity was generally mild with only 4 patients experiencing grade 3 CRS and no one developing grade 3 immune effector cell–associated neurotoxicity syndrome (Supplementary Tables S13–S14). In 7 patients, severe cytopenia was observed after CAR-T treatment (Supplementary Table S14). For patients developing grade 2–3 CRS, there was no correlation to the proportion of CAR-positive T cells in their CAR-T infusion products (Supplementary Fig. S4A) or CAR-T expansion *in vivo* (assessed as the peak CAR values; Supplementary Fig. S4B). On the other hand, patients who experienced grade 2–3 CRS displayed a trend of elevated levels of several proteins in the plasma before CAR-T infusion and also one and three weeks after CAR-T infusion (e.g., IFNγ, TNF, IL12R, CXCL10, CCL3; Supplementary Fig. S4C; Supplementary Tables S8–S10). Seven patients developed low-grade CNS toxicity apart from CRS and these patients displayed no difference in the proportion of CAR-positive T cells in their CAR-T products (Supplementary Fig. S4D) or peak CAR-T values in the blood (Supplementary Fig. S4E) but showed a slight increase in CD27 expression on $CD8^+$CAR-Ts before infusion (Supplementary Fig. S4F). We also observed a trend of a higher proportion of $CD8^+$ cells in the CAR-T product with increased CRS grade (Supplementary Fig. S4G).

scRNA-seq and clustering analysis of the CAR-T products

Response could not be predicted by the level of CAR-T expansion in patients after infusion (Supplementary Fig. S5A) or CAR-T infusion product composition such as the proportion of CAR-positive T cells (Supplementary Fig. S5B) or the CD8/CD4 ratio of CAR-Ts (Supplementary Fig. S5C). We hypothesized that the quality of the individual CAR-T products could influence outcome and therefore investigated the CAR-T infusion products by targeted scRNA-seq. CAR-Ts from the 23 treated patients with lymphoma (the patient with ALL was excluded from the scRNA-seq analysis) were thawed and prepared for targeted scRNA-seq (465 genes) using the BD Rhapsody system (**Fig. 2A**). Dimensionality reduction and unsupervised analysis revealed that T cells from all patients were dispersed across the dimensional space (**Fig. 2B**) and the number of cells that passed QC per patient ranged from approximately 700 to 2,200 cells (**Fig. 2C**). A total of 12 clusters (0–11) were identified by unsupervised clustering (**Fig. 2D**) and cells belonging to each cluster were found in almost all patients (**Fig. 2E**). CD8 versus CD4 expression was determined using scRNA-seq (**Fig. 2F** and **G**) and confirmed by using oligonucleotide-conjugated antibodies (Abseq; Supplementary Fig. S6A and S6B). Importantly, a significant correlation was observed between the proportion of cells identified by scRNA-seq/Abseq and by flow cytometry–based measurements in terms of CD8-positive, CD4-positive, and CAR-positive T cells (Supplementary Fig. S6C–S6E). Clusters 0, 1, 2, 4, 5, 6, 9, 10, and 11 were all defined as CD8 T-cell clusters and clusters 3, 7, and 8 as CD4 T-cell clusters (Supplementary Fig. S6F–S6I). CAR-transduced T cells in the CAR-T infusion products were detected in all clusters (**Fig. 2H**; Supplementary Fig. S6J) and were only associated with a limited number of significant differences in gene expression compared with the non-transduced T cells (Supplementary Fig. S6K). The subsequent analysis was performed specifically on the CAR-transduced T cells. Of note, clusters 10 and 11 were mainly dominated by patients 1 and 25, respectively (Supplementary Fig. S7A) and especially cluster 11 contained very few CAR-Ts (Supplementary Fig. S7B). $CD8^+$CAR-Ts dominated most CAR-T infusion products (Supplementary Fig. S7C).

CAR-T products from responders were dominated by effector $CD8^+$CAR-Ts with high cytotoxic and cytokine signatures

We assessed differences in the CAR-T product transcriptomic signatures and functional states from patients who responded (R) to those that did not respond at 1 month after treatment (**Fig. 3A**). The response at 1 month was selected as the patients had only received one CAR-T infusion at that time point. Comparing $CD8^+$CAR-Ts between responding and non-responding patients showed upregulation of genes associated with effector functions involved in cytotoxicity (*e.g., PRF1, GZMB, GNLY*) and cytokine production (*e.g., CCL3*, *CCL4*, *IFNG*) in responders (**Fig. 3B**; Supplementary Table S7). GO analysis of the DEGs showed that CAR-Ts from responders were enriched for GO terms involving cytolysis, chemokine production, and immune response against tumor cells, whereas CAR-Ts from non-responders were enriched for GO terms involved in negative regulation of T-cell–mediated immunity, signaling, and proliferation (**Fig. 3C**).

Of the 12 clusters identified by unsupervised clustering analysis, nine clusters with $CD8^+$CAR-Ts were identified (**Fig. 3D**). Although cells from both responding and non-responding patients were present in each identified cluster, the distribution of cells from the respective group in each cluster varied (**Fig. 3E** and **F**). Differential gene expression in each cluster and AUCell analysis from previously described gene signatures (cytotoxic, cytokine, cell cycle, exhaustion, and dysfunction; refs. 28–32), were used to define the T-cell subsets and cell-intrinsic functions present in the infusion products (**Fig. 3D**; Supplementary Fig. S8A–S8E; Supplementary Tables S4 and S6). Clusters 1 and 5 were the top two enriched clusters in CAR-T products of responding patients (**Fig. 3D** and **E**). $CD8^+$CAR-Ts in cluster 1 were highly proliferative (*e.g., TOP2A, AURKB, UBE2C, MKI67*) and expressed activation markers, including *MHC-II* and *CD86* and effector molecules *KLRG1* and *NKG7* (**Fig. 3D**; Supplementary Fig. S8D; Supplementary Table S4). The markers expressed in cluster 1 are associated with proliferating short-lived effector $CD8^+$ T cells (33, 34). Cells in cluster 5 expressed *IFNG*, *TNF*, effector molecules (*GZMB, GLNY*), and chemokines (*e.g., CCL1, CCL3, CCL4, XCL1*; **Fig. 3D**;

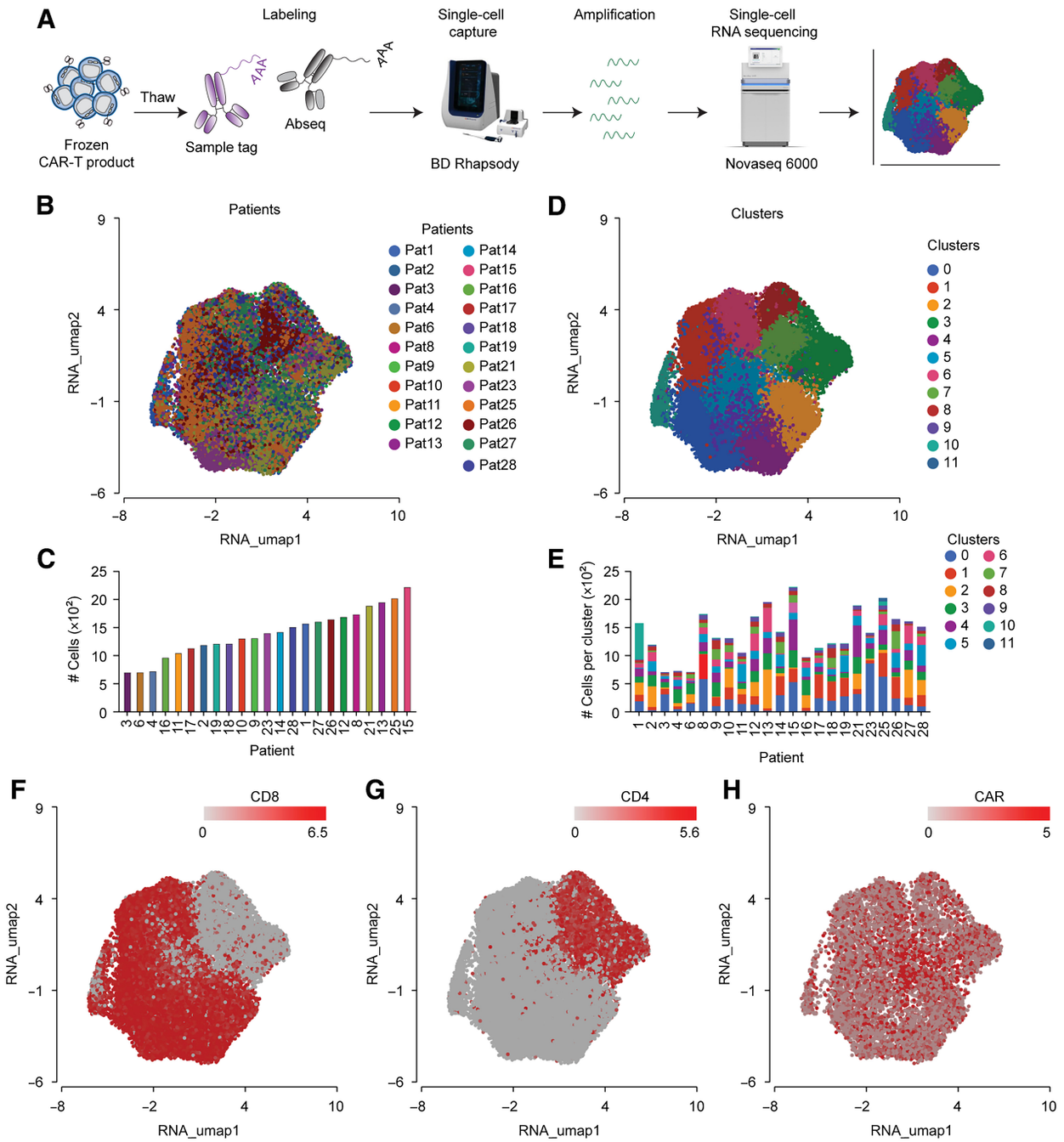

Figure 2.
Overview of single-cell RNA sequencing of the individual CAR-T infusion products. **A,** Schematic overview of the experimental procedure to prepare patient-derived CAR-T products for single-cell RNA sequencing. **B,** An overview of the distribution of cells, which passed quality control (QC), from each patient in the UMAP. **C,** The total number of cells from each patient that passed QC. **D,** UMAP showing the localization of the 12 identified T-cell clusters (0–11). **E,** Bars show total number of cells in each cluster from each patient. Colors reflect the number of cells belonging to each cluster. UMAP displaying the T cells identified as (**F**) $CD8^+$, (**G**) $CD4^+$, and (**H**) CAR^+.

Supplementary Table S4). Expressions of these genes are associated with effector T cells (T_E; ref. 35). In addition, cluster 1 and especially cluster 5 displayed high cytokine secretion and cytotoxic scores and a low dysfunctional score (Supplementary Fig. S8A–S8C). Taken together, responder-enriched clusters (1 and 5) comprised of two distinct effector T-cell subsets, which is in line with our observations that responders display upregulation of gene signatures involved in cytotoxicity and cytokine secretion (**Fig. 3G**). Clusters 0, 6, and 9 had

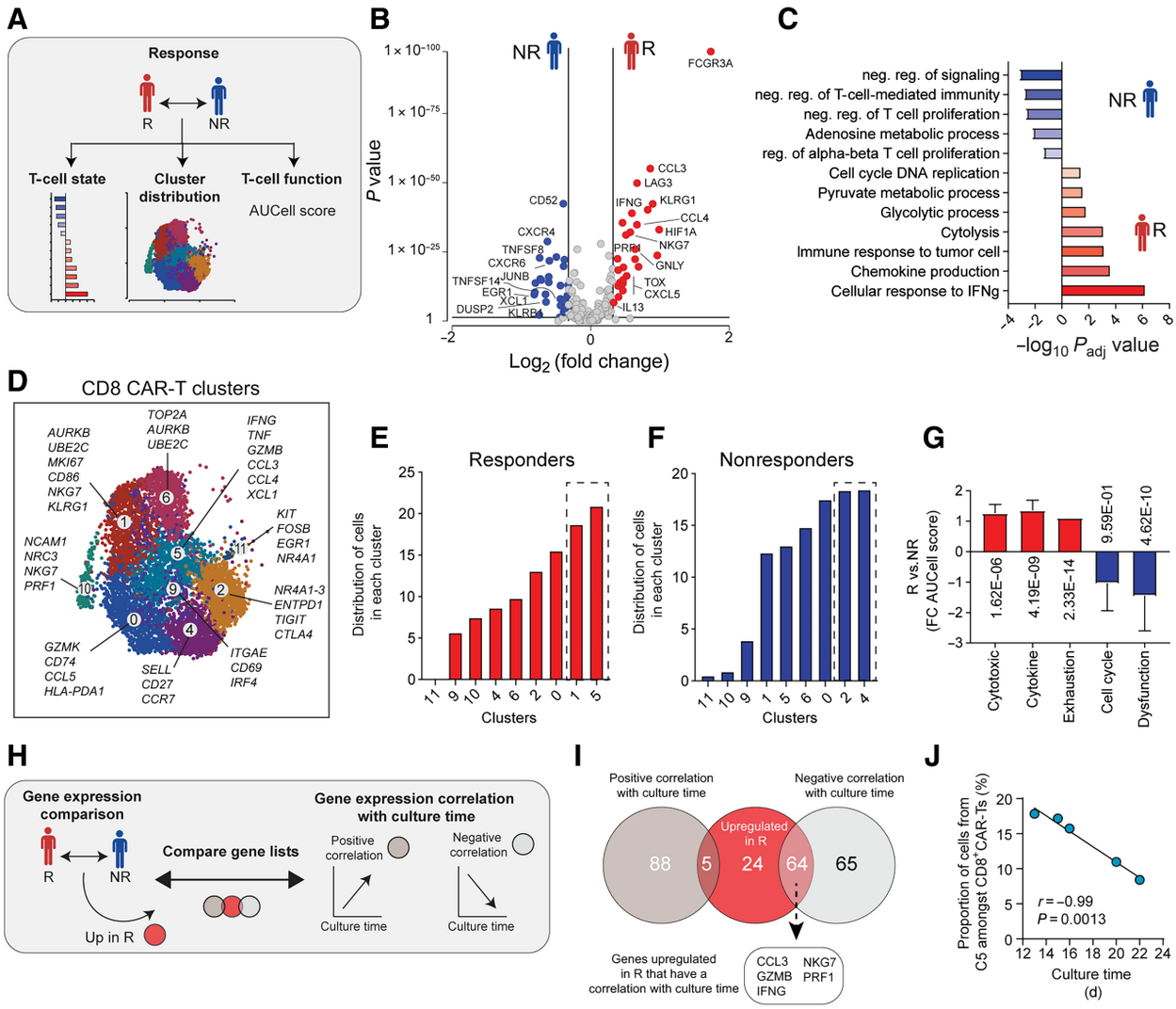

Figure 3.

CD8$^+$CAR-Ts with high cytotoxic and cytokine-gene signatures are associated with response to treatment. **A,** Schematic overview of the analysis performed assessing expression profile and functional score of CD8$^+$CAR-Ts from the infusion product in relation to clinical response at one month after treatment. **B,** Volcano plot depicting differentially expressed genes in responding (R) and non-responding (NR) patients. Red dots represent genes expressed at higher levels in R whereas blue dots represent genes with higher expression levels in NR. The *y*-axis denotes *P* values whereas the *x*-axis shows $\log_2$ fold change. **C,** GO terms analysis of the differentially expressed genes from R and NR. **D,** UMAP showing the CD8$^+$CAR-T clusters generated by unsupervised clustering. Distribution of cells from (**E**) R and (**F**) NR within each CD8$^+$CAR-T cluster. **G,** AUCell scores of functional states compared between R and NR. Welch's ANOVA with Benjamin–Hochberg tests to correct for the FDR value of ≤0.05, was used to assess statistical difference between groups. **H,** Schematic illustration describing the analysis of how genes upregulated in responding patients change in expression (up- or downregulated) with culture time. **I,** Genes with negative (downregulated) and positive (upregulated) correlation with culture time were compared with the genes specifically upregulated in CD8$^+$CAR-Ts from responding patients. **J,** Proportion of CD8$^+$CAR-Ts from cluster 5 in the CAR-T products harvested at different time points during manufacturing. Each dot represents an average of the products collected at each time point. Statistical differences and *R* values were calculated using Pearson correlation.

intermediate representation in the infusion products of both responders and non-responders. Cluster 0 had an intermediate state between effector and exhausted T cells (*GZMK, CD74, CCL5, HLA-DPA1*; **Fig. 3D**; Supplementary Table S4; ref. 36). Cells in cluster 6 were proliferating (*e.g., TOP2A, AURKB, UBE2C, MKI67*) whereas cells in cluster 9 expressed genes associated with tissue resident-memory cells (T_{RM}; *ITGAE, CD69, IRF4*; **Fig. 3D**; Supplementary Table S4; ref. 37). Clusters 2 and 4 were the most represented clusters among non-responding patients (**Fig. 3E** and **F**). Cells in cluster 2 resembled dysfunctional T cells with low cytotoxicity and cytokine scores (Supplementary Fig. S8A–S8C) that expressed genes associated with dysfunction *NR4A1, NR4A2*, and *NR4A3* (38, 39), functional exhaustion markers *ENTPD1* and *TIGIT* (31, 40) and immune checkpoint *CTLA4* (**Fig. 3D**; Supplementary Table S4). In accordance, CD8$^+$CAR-Ts of non-responding patients displayed a dysfunctional gene signature (**Fig. 3G**). Cluster 4 contained central memory-like CD8$^+$CAR-Ts

(T_{CM}; *SELL, CD27, CCR7*; **Fig. 3D**; Supplementary Table S4). Cluster 10 displayed a cytotoxic natural killer T-cell–like signature (*NCAM1, NCR3, KLRC1, KLRC3, NKG7*, and *PRF1*) but about 70% of the cells in this cluster were present in the infusion product of patient 1 (**Fig. 3D**; Supplementary Table S4; Supplementary Fig. S7A) and therefore it is difficult to evaluate the importance of this cluster in relation to response. Cluster 11 comprised of few CAR-Ts (Supplementary Fig. S7C) and was therefore not further evaluated. All $CD8^+$CAR-T clusters had high exhausted T-cell signature (Supplementary Fig. S8E); however, cytokine and cytotoxicity scores of individual clusters positively correlated with exhaustion (Supplementary Fig. S8F–S8H). On the other hand, all T-cell gene signatures had a negative correlation with dysfunction (Supplementary Fig. S8I–S8K). These results indicate that exhaustion observed in $CD8^+$CAR-Ts from responders (**Fig. 3G**) might be a result of activation rather than dysfunction. No AUCell score correlated with cell cycle (Supplementary Fig. S8L–S8O).

Unsupervised clustering of $CD4^+$CAR-Ts resulted in three clusters (3, 7, and 8; Supplementary Table S4). Cells in cluster 3 expressed *SELL*, *LEF1, CD27*, and *IL7R*, which are characteristics of T_{CM}, whereas cells in cluster 7 expressed genes characteristic of the type 1 Th cells profile with cytotoxic capacity (*TBX21, IFNG, CCL3, GZMB, NKG7*, *GNLY*; Supplementary Fig. S9A; Supplementary Table S4). Cells in cluster 8 expressed genes involved in the cell cycle, indicating proliferating cells (*UBEC, TOP2A, AURKB*, *MKI67*; Supplementary Fig. S9A; Supplementary Table S4). There were no striking differences in the proportion of $CD4^+$CAR-Ts in the different clusters (Supplementary Fig. S9B and S9C) and DEGs (Supplementary Fig. S9D; Supplementary Table S16) when comparing responders with non-responders. However, there was a trend to increased proportion of CAR regulatory T-cells in the infusion products of non-responding patients (Supplementary Fig. S9E and S9F), which has been associated with poor response to CD19 CAR-T therapy in patients with DLBCL (41, 42).

In conclusion, CAR-T infusion products with a relatively higher proportion of $CD8^+$CAR-Ts with effector T-cell phenotype-expressing cytotoxic and cytokine secretion factors were associated with better clinical response.

Extended *ex vivo* expansion time during CAR-T production was associated with reduced proportion of effector T cells associated with response

CAR-T infusion products from responders proliferated slightly better during *ex vivo* production compared with CAR-T products from non-responders (Supplementary Fig. S10A and S10B), and were therefore cultured for a shorter time *ex vivo* (Supplementary Fig. S10C). Extended *ex vivo* culture time negatively correlated and fold *ex vivo* expansion positively correlated with the ability of CAR-Ts to proliferate in patients after infusion (Supplementary Fig. S10D and S10E). To determine the impact of culture time on the CAR-T product, correlation between gene expression and *ex vivo* culture time was performed (**Fig. 3H**; Supplementary Fig. S10F). We found 93 genes (*e.g., SLAMF7, CD69, TIGIT, DUSP1*) with a positive correlation and 129 genes (*e.g., CCL3, CCL4, GZMB, GLNY, IFNG, NKG7, PRF1, KLRG1, MKI67*) with a negative correlation with culture time (Supplementary Table S5). Of the 129 genes with negative correlation with extended culture time (decreased expression), 64 genes were also upregulated among responding patients (**Fig. 3I**). Interestingly, several of the commonly found genes are associated with cytotoxicity and cytokine secretion, and products with longer culture time during CAR-T manufacturing had a lower proportion of cells belonging to the responder-enriched effector-like $CD8^+$CAR-Ts (cluster 5; **Fig. 3I** and **J**). Among genes upregulated in $CD8^+$CAR-Ts from non-responders, most genes had a positive correlation with extended culture time (increased expression; Supplementary Fig. S10G).

In summary, the *ex vivo* culture time during CAR-T production negatively impacts expression of cytotoxic and cytokine secretion signatures. A shorter CAR-T production could be desirable to maintain the effector $CD8^+$CAR-T subset correlating with response in this study.

Increased polyfunctional heterogeneity of the CAR-T product was associated with clinical response

Given that the infusion CAR-T products from the responders had more effector T cells, we next assessed the polyfunctionality of our CAR-T products, as it is known to be a predictor for clinical outcome (24). scPSI values of CAR-Ts were defined as CAR-Ts co-expressing two or more markers per cell from a prespecified categorical list, linked to the expression level of the respective gene (**Fig. 4A**). The majority of the $CD8^+$CAR-Ts in the infusion product co-expressed 2 or 3 genes whereas few cells co-expressed 4 or more genes (**Fig. 4B**). Expression of individual genes in individual patients is displayed in Supplementary Fig. S11. Overall, CAR-T products had a wide range of scPSI values, with a majority of the CAR-Ts having a chemoattractive expression profile followed by an effector expression profile (**Fig. 4C**). The total fraction of polyfunctional CAR-Ts (**Fig. 4D**) and the global average scPSI (**Fig. 4E**) were higher in CAR-T infusion products from responders compared with non-responders. The fraction of polyfunctional cells (**Fig. 4F**) and scPSI (**Fig. 4G**) did not change with longer *ex vivo* expansion time of CAR-Ts. However, the scPSI values of CAR-Ts from responders were always higher than non-responders irrespective of culture time. Responders had a higher fraction of polyfunctional $CD4^+$CAR-Ts but lower scPSI compared with non-responders (Supplementary Fig. S12A–S12D). The scPSI (Supplementary Fig. S12E) and fraction of polyfunctional (Supplementary Fig. S11F) cells among $CD4^+$CAR-Ts had a trend to decrease with extended culture time but no difference was observed between responders and non-responders (Supplementary Fig. S12E and S12F). In conclusion, our results show that a combination of fraction of polyfunctional $CD8^+$CAR-Ts and the cytokine expression levels of these cells in the product are associated with clinical response.

The importance of effector $CD8^+$CAR-Ts for response was verified phenotypically

Next, we compared the cellular functional states within CAR-T products from responders and non-responders at the protein level by flow cytometry (**Fig. 5A**). CAR-Ts in the infusion product of non-responders had increased surface protein expression of the early T-cell dysfunction marker CD40L (**Fig. 5B**; ref. 30) and the immune checkpoint receptor TIM-3 (**Fig. 5C**). Furthermore, $CD8^+$CAR-Ts from responders had a higher proportion of $CD45RA^+CCR7^-$ T_E CAR-Ts (**Fig. 5D** and **E**), whereas patients with poor response had higher proportion of $CD45RA^-CCR7^-$ effector memory CAR-Ts (T_{EM}; **Fig. 5E**). There were no differences in the frequencies of $CD45RA^-CCR7^+$ T_{CM} CAR-Ts but a trend towards increased proportion of naïve T cells (T_N) among responders (**Fig. 5E**). In addition, unstimulated $CD45RA^+CCR7^-$ T_E CAR-Ts of responders expressed higher levels of chemokines (CCL4, CCL3) and cytotoxic molecules (GZMB, PRF1; **Fig. 5F**). No IFNγ or TNFα expression was observed in unstimulated T_E CAR-Ts (data not shown). This supports the importance of effector $CD8^+$CAR-Ts for clinical response observed in the scRNA-seq data.

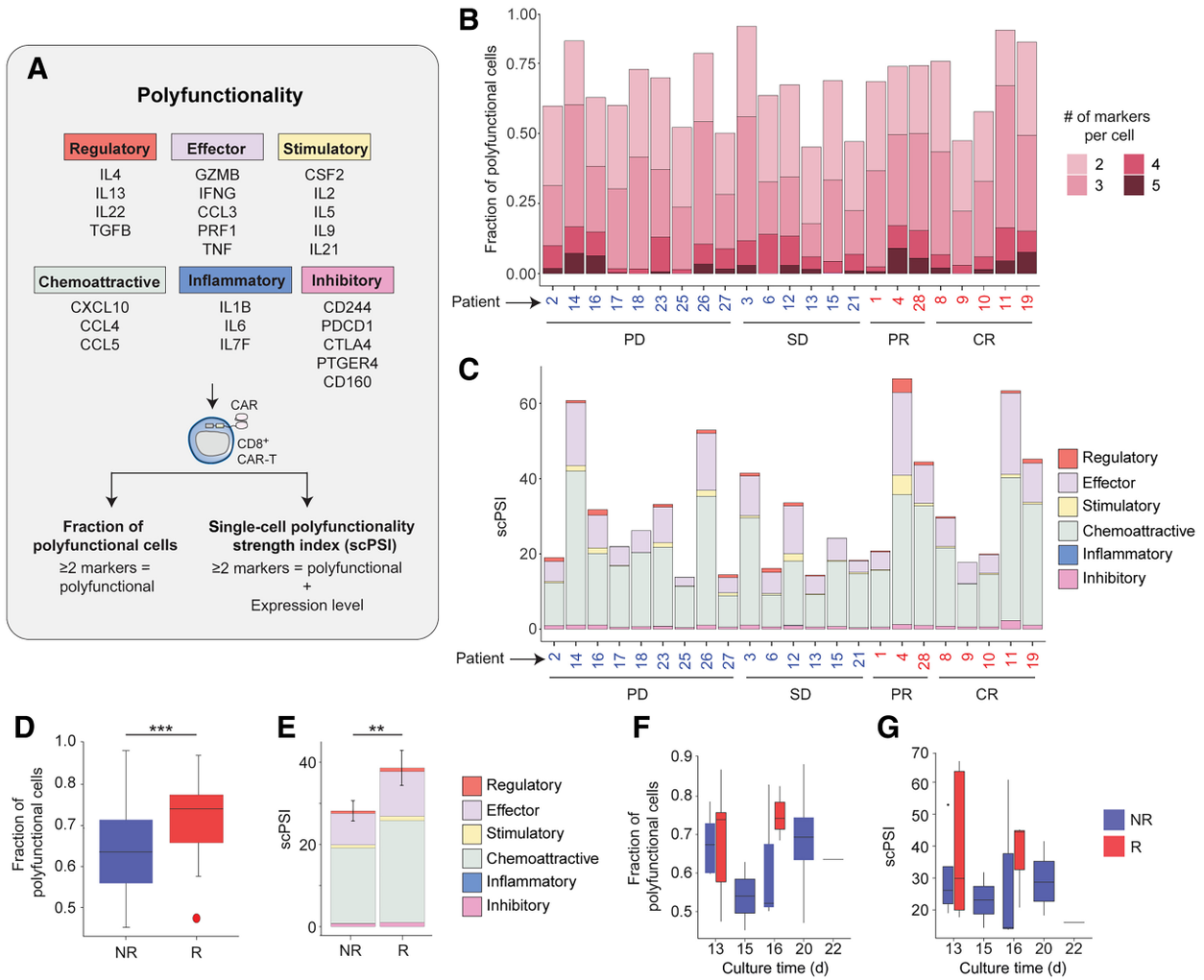

Figure 4.

Association between single-cell polyfunctionality strength index (scPSI) of CD8$^+$CAR-Ts with clinical response and *ex vivo* expansion time. **A,** Polyfunctionality of CAR-Ts was measured as scPSI using a prespecified panel of key immunologically relevant gene markers across the categories: regulatory, effector, stimulatory, chemoattractive, inflammatory, and inhibitory. **B,** Fraction of CD8$^+$CAR-Ts positive for two or more genes (specified in **A**) across all patients. **C,** scPSI, according to polyfunctionality category in **A**, of CD8$^+$CAR-Ts for all patients. **D,** Fraction of CD8$^+$CAR-Ts positive for two or more genes from responders (R) versus non-responders (NR). The difference in ratio of polyfunctional versus non-polyfunctional cells between the two groups was determined using the Fisher's exact test (*P* value <2.2E−16). **E,** scPSI, according to polyfunctionality category in **A**, of CD8$^+$CAR-Ts from R versus NR. The difference between scPSI across the two groups was determined according to the bootstrap *P* value ($P = 0.016$). **F,** Fraction of CD8$^+$CAR-Ts positive for two or more genes from R versus NR plotted against culture time. **G,** scPSI of CD8$^+$CAR-Ts from R versus NR plotted against culture time. R ($n = 8$) and NR ($n = 15$). **, $P \leq 0.01$; ***, $P \leq 0.001$.

After exposure to CD19$^+$ tumor cells (**Fig. 5G**; Supplementary Fig. S13A), CAR-Ts from both responders and non-responders upregulated CD69 (Supplementary Fig. S13B) and death receptor CD95 (Fas; Supplementary Fig. S13C), and secreted IFNγ (Supplementary Fig. S13D). Furthermore, a significantly higher proportion of CD45RA$^+$CCR7$^-$ T_E CAR-Ts from responders expressed cytotoxic molecules (IFNγ, TNFα, and PRF1) and a trend toward increased proportion of cells expressing chemokines (CCL3, CCL4, and CCL5) was observed (**Fig. 5H**), indicating activation in response to tumor cells. In addition, CAR-Ts from responders upregulated CD27, a member of the TNF-receptor superfamily (Supplementary Fig. S13E), and the immune checkpoint receptor TIM-3 (Supplementary Fig. S13G) after exposure to tumor cells. In contrast, CAR-Ts from non-responders upregulated CD25 (IL2Rα) after stimulation (Supplementary Fig. S13F). No difference in expression of CD40L or PD1 was observed between responders and non-responders after *in vitro* stimulation with CD19$^+$ tumor cells (Supplementary Fig. S13H and S13I). A summary of expression of different T-cell activation and exhaustion markers in the CAR-T infusion products before or after overnight stimulation with tumor cells are shown in Supplementary Fig. S13J.

In summary, CAR-T infusion products from responders have more CD8$^+$ T_E CAR-Ts and upon antigen-stimulation (co-cultured with tumor cells), a higher proportion of these cells express the effector molecules IFNγ and TNFα. Furthermore, after stimulation CAR-Ts

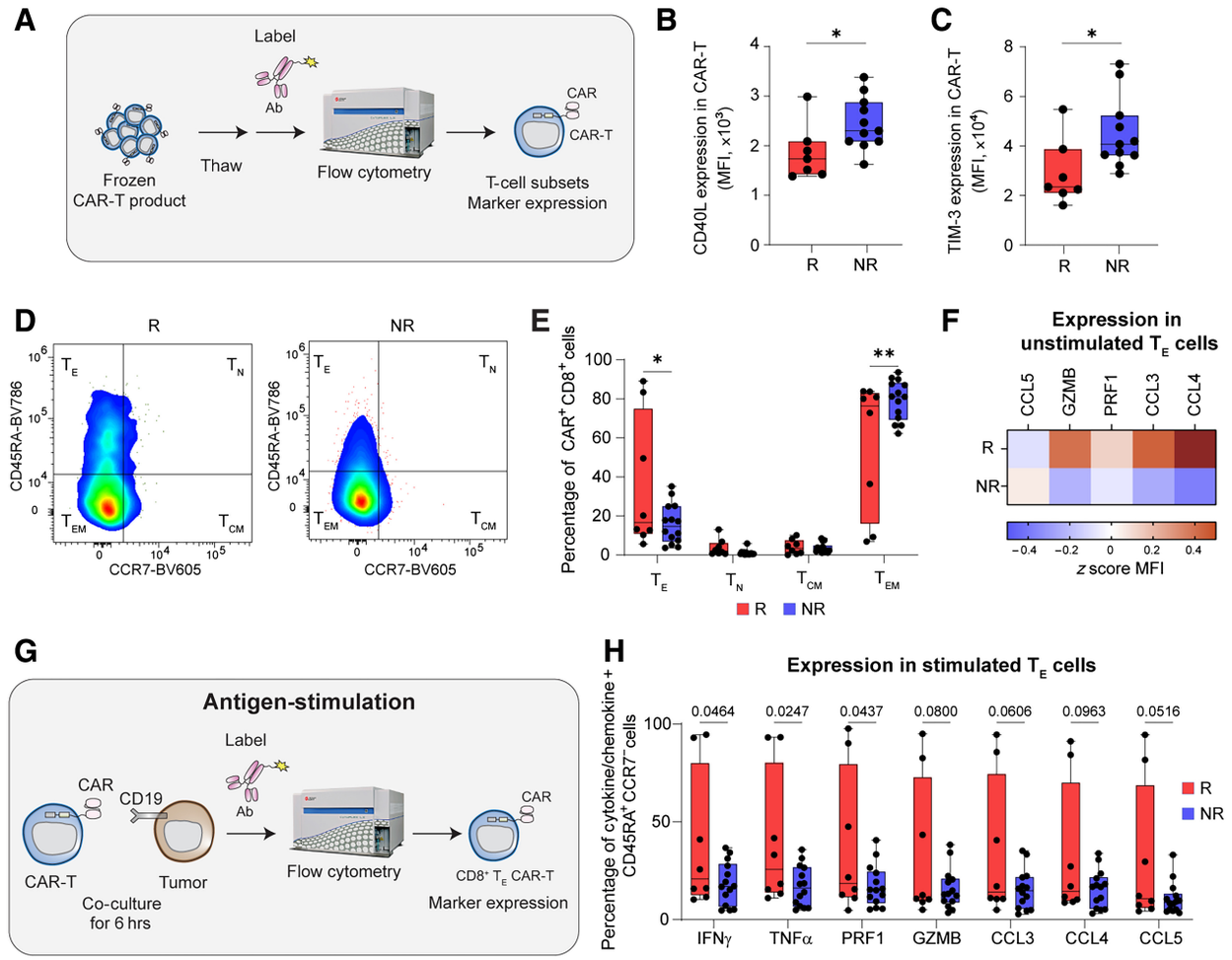

Figure 5.

Effector CD8$^+$CAR-Ts with high expression of cytotoxic molecules upon antigen stimulation associate with response. **A,** Schematic illustration of *in vitro* characterization of CAR-T infusion products at the protein level by flow cytometry. Mean fluorescence intensity (MFI) of (**B**) CD40L and (**C**) TIM-3 expression on CAR-Ts from responders (R; $n = 7$) and non-responders (NR; $n = 11$). An unpaired *t* test was used to compare between groups (*, $P \le 0.05$). **D,** Representative plot and gating strategy for gating out T effector (T_E, CD45RA$^+$CCR7$^-$), T naïve (T_N, CD45RA$^+$CCR7$^+$), T central memory (T_{CM}, CD45RA$^-$CCR7$^+$), and T effector memory (T_{EM}, CD45RA$^-$CCR7$^-$) CD8$^+$CAR-Ts. **E,** The percentage of T_E, T_N, T_{CM}, and T_{EM} of CD8$^+$CAR-Ts in R ($n = 8$) and NR ($n = 14$). Fisher's least significance difference (LSD) test was used to compare between groups (*, $P \le 0.05$; **, $P < 0.01$). **F,** Average z-score of marker expression on CD8$^+$ T_E CAR-Ts from R ($n = 8$) and NR ($n = 14$) before antigen stimulation. **G,** Illustration of experimental setup to assess marker expression after co-culture with CD19$^+$ tumor cells. **H,** Proportion of CD8$^+$ T_E CAR-Ts expressing IFNγ, TNFα, PRF1, GZMB, CCL3, CCL4, and CCL5 from R ($n = 8$) and NR ($n = 14$) after co-culture with CD19$^+$ tumor cells. Each dot represents data from one donor co-culture and data are shown as boxplots with whiskers, indicating Min and Max points. Fisher's LSD test was used to compare between groups (*, $P \le 0.05$).

from responders had higher CD27 and lower CD25 expression than non-responders.

Discussion

CD19 CAR-T therapy has emerged as a potent treatment option for patients with advanced B-cell malignancies (1–3). However, the response rates differ across the various malignancies and there are still many patients who do not benefit from treatment with CD19 CAR-Ts (8). The response rate to the third-generation CD19 CAR-Ts used in this study was lower than what has been observed for lymphoma patients using second-generation CD19 CAR-Ts; however, a lower level of toxicity was also observed in this study (8). Although third-generation CARs promote enhanced T-cell activation (19, 43) and survival (43, 44) compared with second-generation CARs, no enhanced clinical efficacy has been reported. We observed poor persistence of third-generation CAR-Ts after infusion; therefore, it is not surprising that a lower response was observed compared with studies using second-generation CARs. It is important to point out that we used a milder lymphodepletion regimen compared with most other protocols (7, 9), which could contribute to the lower engraftment of CAR-Ts in the patients and poorer response.

Several factors can influence the response to CAR-T therapy, including CAR design, characteristics of the infusion product, preconditioning, number of doses, etc. Like most CD19-directed CAR-Ts, including second-generation CAR-T therapies axicabtagene ciloleucel

(axi-cel) and tisagenlecleucel (tisa-cel), our CAR-Ts use the FMC63 clone as the CD19-targeting moiety. However, the spacer region is derived from immunoglobulin G1 CH2CH3 domains in contrast with axi-cel, which has a hinge and transmembrane domain derived from CD8a and tisa-cel, which uses CD28. Furthermore, we observed a low response rate despite dual CAR-T infusion in a majority of the patients as observed in other studies (4, 45). The lack of a survival benefit in patients receiving dual CAR-T infusions was likely due to the limited engraftment and expansion of CAR-Ts upon re-infusion (45, 46). Responses observed after a second infusion are due to either administration of higher CAR-T dose compared with the first infusion (47) or additional lymphodepletion before infusion (46), none of which were applied in this study. Despite having a small patient cohort with heterogenous clinical procedures, CRP levels and the MTV (27) before treatment were associated with OS and PFS. This is in line with previous studies where both increased CRP levels and tumor volume has been found to have a predictive value for early progression (48) and response to CAR-T treatment (49, 50).

The status of the starting material for CAR-T manufacturing (14, 15) and the quality of CAR-T infusion product significantly influences efficacy (13, 50). Therefore, we investigated whether discrete cellular states of the infused CAR-Ts were associated with response to therapy in patients with B-cell lymphoma. We found that $CD8^+$CAR-Ts from the infusion products of responding patients had an enrichment of effector-like T cells expressing activation and effector molecules. However, a higher proportion of cells expressing activation and effector molecules in axi-cel pre-infusion products was associated with therapeutic failure (13). In other studies, a higher proportion of cells expressing a T_{CM} signature in the infusion product has been associated with clinical response (13, 41, 51). T_{CM} cells were almost completely absent in our study, most likely due to long-term manufacturing in the presence of IL2, skewing cells toward an effector phenotype (52–54). Because of factors such as different CAR-T manufacturing protocol and CAR design it is therefore difficult to directly compare CAR-T infusion products from different studies. This has become evident as cells from infusion products of axi-cel and tisa-cel, incorporating different co-stimulatory domains, have different phenotypes suggesting that the CAR design influences the T-cell phenotype (41). The third-generation CAR used here includes both 4–1BB and CD28 co-stimulatory domains and the infusion product has a completely different profile compared with previously published studies (13, 41). Importantly, gene expression phenotypes associated with response to axi-cel in one study could not be replicated in another study (13, 41). Considering these findings, it is of great importance to evaluate which infusion product characteristics are associated with response in studies using different CAR constructs, manufacturing methods, etc., individually to enable accurate prediction of response.

It is not only the frequency of T-cell subsets in the CAR-T infusion product that influences the response but rather the cell-intrinsic functions of these subsets such as cytotoxic potency of T_E CAR-Ts and proliferation of T_{CM} CAR-Ts (24, 51). Importantly, in line with this we also found that high polyfunctionality in infusion product T cells was associated with clinical response (24). Furthermore, cells associated with response displayed cytotoxic and cytokine secretion signatures and low dysfunction. We hypothesize that in the lack of T_{CM} CAR-Ts, previously associated with response (13, 41), in this study, the T_E CAR-Ts with highly functional characteristics might be important to promote a clinical response. $CD8^+$CAR-Ts overrepresented in non-responding patients on the other hand were less polyfunctional and displayed an elevated T-cell dysfunction gene signature (24, 51). T-cell dysfunction is associated with an inability to exert effector functions such as secretion of cytotoxic molecules and cytokines (55). In line with those findings, effector $CD8^+$CAR-Ts from infusion products of non-responding patients secreted less effector molecules upon stimulation compared with responding patients in our study.

Manufacturing time and culture conditions during CAR-T production are important determinants of the status of the final CAR-T infusion product (52, 54). The proportion of responder-enriched T_E CAR-Ts in infusion products decreased with extended culture time. This suggests that a short culture time was important to maintain this CAR-T subset. Low cell doubling time during CAR-T manufacturing has been associated with a lower response rate and lower ability of the CAR-Ts to expand in patients after infusion (50). In line with these findings, we also observed a correlation between CAR-T expansion *ex vivo* and *in vivo*. Cell doubling time in culture was suggested as a measure of T-cell fitness and was associated with the apheresis product used to produce CAR-Ts (50). However, further studies would be needed to determine whether the observed phenotypes in the cell pool and expansion of CAR-Ts in our study can be attributed to the quality of the starting material.

In summary, we found that $CD8^+$CAR-Ts with high polyfunctional index, cytotoxic and cytokine secretion signature/phenotype, and low dysfunction phenotype were associated with response to CAR-T treatment.

Authors' Disclosures

T. Lövgren reports grants from Lokon Pharma AB and Vivolux AB outside the submitted work. H. Ahlström reports grants from Swedish Cancer Society during the conduct of the study. A. Loskog reports personal fees from Lokon Pharma, Vivolux, Repos Pharma, Aros Biotech, and Tanea Medical; grants from Lokon Pharma; and other support from Nexttobe, Almo Alo, Lynxalo, and Promegranade outside the submitted work. In addition, A. Loskog also reports patents 10973875 and 8685640 issued. G. Enblad reports grants from Swedish Cancer Foundation during the conduct of the study. M. Essand is co-founder and Chief Scientific Officer of Elicera Therapeutics, which is active within the CAR-T cell space; the CAR-T cells and the retroviral construct used to produce the CAR-T cells in this publication are outside any intellectual property and activity of Elicera Therapeutics. No disclosures were reported by the other authors.

Authors' Contributions

T. Sarén: Conceptualization, data curation, formal analysis, validation, investigation, visualization, methodology, writing–original draft, project administration, writing–review and editing. **M. Ramachandran:** Conceptualization, data curation, formal analysis, validation, investigation, visualization, methodology, writing–original draft, project administration, writing–review and editing. **G. Gammelgård:** Data curation, writing–review and editing. **T. Lövgren:** Conceptualization, data curation, project administration, writing–review and editing. **C. Mirabello:** Software, formal analysis, methodology, writing–review and editing. **Å.K. Björklund:** Software, formal analysis, supervision, methodology, writing–review and editing. **K. Wikström:** Data curation, writing–review and editing. **J. Hashemi:** Project administration. **E. Freyhult:** Data curation, software, formal analysis, writing–review and editing. **H. Ahlström:** Conceptualization, data curation, formal analysis, writing–review and editing. **R.-M. Amini:** Conceptualization. **H. Hagberg:** Conceptualization, data curation, investigation. **A. Loskog:** Conceptualization, supervision, funding acquisition, investigation, writing–review and editing. **G. Enblad:** Conceptualization, data curation, supervision, funding acquisition, writing–review and editing. **M. Essand:** Conceptualization, data curation, supervision, funding acquisition, writing–original draft, writing–review and editing.

Acknowledgments

The authors would like to thank research nurses and staff at the clinical research and development unit at Uppsala University Hospital for assistance in the clinical trial management. The authors also wish to thank the faculty and staff at the Center for Cell and Gene Therapy at Baylor College of Medicine for vector development and manufacture. We acknowledge the BioVis Core Facility (Uppsala University) for

assistance with flow sorting, and the SNP&SEQ Technology Platform (Uppsala University) for performing the illumina RNA sequencing. This work was supported by research grants from the Swedish Research Council: 2019–01326 (to M. Essand) and 2019–01721 (to A. Loskog); the Swedish Cancer Society: 19 0184Pj (to M. Essand), 20 0756 PjF (to A. Loskog), and 20 1303 PjF (to G. Enblad); AFA Insurance for regenerative medicine (to A. Loskog and M. Essand); Lions Cancer Fund at Uppsala University Hospital (to G. Enblad); and the Swedish State Support for Clinical Research (to G. Enblad). M. Ramachandran was supported by a postdoctoral grant from Barncancerfonden (TJ 2019-0014). C. Mirabello and Å.K. Björklund are financially supported by the Knut and Alice Wallenberg Foundation as part of the National Bioinformatics Infrastructure Sweden at SciLifeLab (KAW 2017.0003).

The publication costs of this article were defrayed in part by the payment of publication fees. Therefore, and solely to indicate this fact, this article is hereby marked "advertisement" in accordance with 18 USC section 1734.

Note

Supplementary data for this article are available at Clinical Cancer Research Online (http://clincancerres.aacrjournals.org/).

Received January 20, 2023; revised June 22, 2023; accepted August 2, 2023; published first August 4, 2023.

References

1. Schuster SJ, Svoboda J, Chong EA, Nasta SD, Mato AR, Anak Ö, et al. Chimeric antigen receptor T cells in refractory B-cell lymphomas. N Engl J Med 2017;377:2545–54.
2. Neelapu SS, Locke FL, Bartlett NL, Lekakis LJ, Miklos DB, Jacobson CA, et al. Axicabtagene ciloleucel CAR T-cell therapy in refractory large B-cell lymphoma. N Engl J Med 2017;377:2531–44.
3. Abramson JS, Palomba ML, Gordon LI, Lunning MA, Wang M, Arnason J, et al. Lisocabtagene maraleucel for patients with relapsed or refractory large B-cell lymphomas (TRANSCEND NHL 001): a multicentre seamless design study. Lancet 2020;396:839–52.
4. Turtle CJ, Hanafi L-A, Berger C, Hudecek M, Pender B, Robinson E, et al. Immunotherapy of non-Hodgkin's lymphoma with a defined ratio of $CD8^+$ and $CD4^+$ CD19-specific chimeric antigen receptor-modified T cells. Sci Transl Med 2016;8:355ra116.
5. Davila ML, Riviere I, Wang X, Bartido S, Park J, Curran K, et al. Efficacy and toxicity management of 19–28z CAR T-cell therapy in B-cell acute lymphoblastic leukemia. Sci Transl Med 2014;6:224ra225.
6. Maude SL, Laetsch TW, Buechner J, Rives S, Boyer M, Bittencourt H, et al. Tisagenlecleucel in children and young adults with B-cell lymphoblastic leukemia. N Engl J Med 2018;378:439–48.
7. Locke FL, Miklos DB, Jacobson CA, Perales M-A, Kersten M-J, Oluwole OO, et al. Axicabtagene ciloleucel as second-line therapy for large B-cell lymphoma. N Engl J Med 2022;386:640–54.
8. Majzner RG, Mackall CL. Clinical lessons learned from the first leg of the CAR T-cell journey. Nat Med 2019;25:1341–55.
9. Neelapu SS, Dickinson M, Munoz J, Ulrickson ML, Thieblemont C, Oluwole OO, et al. Axicabtagene ciloleucel as first-line therapy in high-risk large B-cell lymphoma: the phase 2 ZUMA-12 trial. Nat Med 2022;28:735–42.
10. Park JH, Rivière I, Gonen M, Wang X, Sénéchal B, Curran KJ, et al. Long-term follow-up of CD19 CAR therapy in acute lymphoblastic leukemia. N Engl J Med 2018;378:449–59.
11. Maude SL, Frey N, Shaw PA, Aplenc R, Barrett DM, Bunin NJ, et al. Chimeric antigen receptor T cells for sustained remissions in leukemia. N Engl J Med 2014;371:1507–17.
12. Schuster SJ, Bishop MR, Tam CS, Waller EK, Borchmann P, McGuirk JP, et al. Tisagenlecleucel in adult relapsed or refractory diffuse large B-cell lymphoma. N Engl J Med 2019;380:45–56.
13. Deng Q, Han G, Puebla-Osorio N, Ma MCJ, Strati P, Chasen B, et al. Characteristics of anti-CD19 CAR T-cell infusion products associated with efficacy and toxicity in patients with large B-cell lymphomas. Nat Med 2020;26:1878–87.
14. Finney OC, Brakke H, Rawlings-Rhea S, Hicks R, Doolittle D, Lopez M, et al. CD19 CAR T-cell product and disease attributes predict leukemia remission durability. J Clin Invest 2019;129:2123–32.
15. Fraietta JA, Lacey SF, Orlando EJ, Pruteanu-Malinici I, Gohil M, Lundh S, et al. Determinants of response and resistance to CD19 chimeric antigen receptor (CAR) T-cell therapy of chronic lymphocytic leukemia. Nat Med 2018;24:563–71.
16. Enblad G, Karlsson H, Gammelgård G, Wenthe J, Lövgren T, Amini RM, et al. A phase I/IIa trial using CD19-targeted third-generation CAR T cells for lymphoma and leukemia. Clin Cancer Res 2018;24:6185–94.
17. Eriksson E, Wenthe J, Irenaeus S, Loskog A, Ullenhag G. Gemcitabine reduces MDSCs, Tregs and TGFbeta-1 while restoring the Teff/Treg ratio in patients with pancreatic cancer. J Transl Med 2016;14:282.
18. Johnson SA, Kumar A, Matasar MJ, Schoder H, Rademaker J. Imaging for staging and response assessment in lymphoma. Radiology 2015;276:323–38.
19. Karlsson H, Svensson E, Gigg C, Jarvius M, Olsson-Strömberg U, Savoldo B, et al. Evaluation of intracellular signaling downstream chimeric antigen receptors. PLoS ONE 2015;10:e0144787.
20. Shum EY, Walczak EM, Chang C, Fan HC. Quantitation of mRNA transcripts and proteins using the BD rhapsody single-cell analysis system. Adv Exp Med Biol 2019;1129:63–79.
21. Hao Y, Hao S, Andersen-Nissen E, Mauck WM, Zheng S, Butler A, et al. Integrated analysis of multimodal single-cell data. Cell 2021;184:3573–87.
22. Arya S, Mount DM, Netanyahu NS, Silverman R, Wu AY. An optimal algorithm for approximate nearest neighbor searching in fixed dimensions. J Acm 1998;45:891–923.
23. Aibar S, González-Blas CB, Moerman T, Huynh-Thu VA, Imrichova H, Hulselmans G, et al. SCENIC: single-cell regulatory network inference and clustering. Nat Methods 2017;14:1083–6.
24. Rossi J, Paczkowski P, Shen Y-W, Morse K, Flynn B, Kaiser A, et al. Preinfusion polyfunctional anti-CD19 chimeric antigen receptor T cells are associated with clinical outcomes in NHL. Blood 2018;132:804–14.
25. Bates D, Mächler M, Bolker B, Walker S. Fitting linear mixed-effects models using lme4. J Stat Softw 2015;67:1–48.
26. Lenth RV. emmeans: estimated marginal means, aka least-squares means. 2023. Available from: https://github.com/rvlenth/emmeans.
27. Sjöholm T, Korenyushkin A, Gammelgård G, Sarén T, Lövgren T, Loskog A, et al. Whole body FDG PET/MR for progression free and overall survival prediction in patients with relapsed/refractory large B-cell lymphomas undergoing CAR T-cell therapy. Cancer Imaging 2022;22:76.
28. Szabo PA, Levitin HM, Miron M, Snyder ME, Senda T, Yuan J, et al. Single-cell transcriptomics of human T cells reveals tissue and activation signatures in health and disease. Nat Commun 2019;10:4706.
29. Dominguez D, Tsai Y-H, Gomez N, Jha DK, Davis I, Wang Z. A high-resolution transcriptome map of cell cycle reveals novel connections between periodic genes and cancer. Cell Res 2016;26:946–62.
30. Philip M, Fairchild L, Sun L, Horste EL, Camara S, Shakiba M, et al. Chromatin states define tumour-specific T-cell dysfunction and reprogramming. Nature 2017;545:452–6.
31. Sade-Feldman M, Yizhak K, Bjorgaard SL, Ray JP, de Boer CG, Jenkins RW, et al. Defining T-cell states associated with response to checkpoint immunotherapy in melanoma. Cell 2018;175:998–1013.
32. Schietinger A, Philip M, Krisnawan VE, Chiu EY, Delrow JJ, Basom RS, et al. Tumor-specific T-cell dysfunction is a dynamic antigen-driven differentiation program initiated early during tumorigenesis. Immunity 2016;45:389–401.
33. Joshi NS, Cui W, Chandele A, Lee HK, Urso DR, Hagman J, et al. Inflammation directs memory precursor and short-lived effector CD8(+) T-cell fates via the graded expression of T-bet transcription factor. Immunity 2007;27:281–95.
34. Ng SS, De Labastida Rivera F, Yan J, Corvino D, Das I, Zhang P, et al. The NK cell granule protein NKG7 regulates cytotoxic granule exocytosis and inflammation. Nat Immunol 2020;21:1205–18.
35. Eberlein J, Davenport B, Nguyen TT, Victorino F, Jhun K, van der Heide V, et al. Chemokine signatures of pathogen-specific T cells I: effector T cells. J Immunol 2020;205:2169–87.
36. Liu F, Liu W, Sanin DE, Jia G, Tian M, Wang H, et al. Heterogeneity of exhausted T cells in the tumor microenvironment is linked to patient survival following resection in hepatocellular carcinoma. Oncoimmunology 2020;9:1746573.
37. Kumar BV, Ma W, Miron M, Granot T, Guyer RS, Carpenter DJ, et al. Human tissue-resident memory T cells are defined by core transcriptional and functional signatures in lymphoid and mucosal sites. Cell Rep 2017;20:2921–34.

38. Liu X, Wang Y, Lu H, Li J, Yan X, Xiao M, et al. Genome-wide analysis identifies NR4A1 as a key mediator of T-cell dysfunction. Nature 2019;567:525–9.
39. Chen J, López-Moyado IF, Seo H, Lio C-WJ, Hempleman LJ, Sekiya T, et al. NR4A transcription factors limit CAR T-cell function in solid tumours. Nature 2019;567:530–4.
40. Wei YY, Fan J, Shan MX, Yin DD, Wang LL, Ye W, et al. TIGIT marks exhausted T cells and serves as a target for immune restoration in patients with chronic HBV infection. Am J Transl Res 2022;14:942–54.
41. Haradhvala NJ, Leick MB, Maurer K, Gohil SH, Larson RC, Yao N, et al. Distinct cellular dynamics associated with response to CAR-T therapy for refractory B-cell lymphoma. Nat Med 2022;28:1848–59.
42. Good Z, Spiegel JY, Sahaf B, Malipatlolla MB, Ehlinger ZJ, Kurra S, et al. Post-infusion CAR T(reg) cells identify patients resistant to CD19-CAR therapy. Nat Med 2022;28:1860–71.
43. Zhong XS, Matsushita M, Plotkin J, Riviere I, Sadelain M. Chimeric antigen receptors combining 4–1BB and CD28 signaling domains augment PI3kinase/AKT/Bcl-XL activation and $CD8^+$ T-cell–mediated tumor eradication. Mol Ther 2010;18:413–20.
44. Ramos CA, Rouce R, Robertson CS, Reyna A, Narala N, Vyas G, et al. *In vivo* fate and activity of second- versus third-generation CD19-specific CAR-T cells in B-cell non-Hodgkin's lymphomas. Mol Ther 2018;26:2727–37.
45. Gardner RA, Finney O, Annesley C, Brakke H, Summers C, Leger K, et al. Intent-to-treat leukemia remission by CD19 CAR T cells of defined formulation and dose in children and young adults. Blood 2017;129:3322–31.
46. Holland EM, Molina JC, Dede K, Moyer D, Zhou T, Yuan CM, et al. Efficacy of second CAR-T (CART2) infusion limited by poor CART expansion and antigen modulation. J Immunother Cancer 2022;10:e004483.
47. Gauthier J, Bezerra ED, Hirayama AV, Fiorenza S, Sheih A, Chou CK, et al. Factors associated with outcomes after a second CD19-targeted CAR T-cell infusion for refractory B-cell malignancies. Blood 2021;137:323–35.
48. Vercellino L, Di Blasi R, Kanoun S, Tessoulin B, Rossi C, D'Aveni-Piney M, et al. Predictive factors of early progression after CAR T-cell therapy in relapsed/refractory diffuse large B-cell lymphoma. Blood Adv 2020;4:5607–15.
49. Liu Y, Jie X, Nian L, Wang Y, Wang C, Ma J, et al. A combination of pre-infusion serum ferritin, CRP and IL6 predicts outcome in relapsed/refractory multiple myeloma patients treated with CAR-T cells. Front Immunol 2023;14:1169071.
50. Locke FL, Rossi JM, Neelapu SS, Jacobson CA, Miklos DB, Ghobadi A, et al. Tumor burden, inflammation, and product attributes determine outcomes of axicabtagene ciloleucel in large B-cell lymphoma. Blood Adv 2020;4:4898–911.
51. Kirouac DC, Zmurchok C, Deyati A, Sicherman J, Bond C, Zandstra PW. Deconvolution of clinical variance in CAR T-cell pharmacology and response. Nat Biotechnol 2023 Feb 27 [Epub ahead of print].
52. Zhang X, Lv X, Song Y. Short-term culture with IL-2 is beneficial for potent memory chimeric antigen receptor T-cell production. Biochem Biophys Res Commun 2018;495:1833–8.
53. Kaartinen T, Luostarinen A, Maliniemi P, Keto J, Arvas M, Belt H, et al. Low interleukin-2 concentration favors generation of early memory T cells over effector phenotypes during chimeric antigen receptor T-cell expansion. Cytotherapy 2017;19:689–702.
54. Meyran D, Zhu JJ, Butler J, Tantalo D, MacDonald S, Nguyen TN, et al. T (STEM)-like CAR-T cells exhibit improved persistence and tumor control compared with conventional CAR-T cells in preclinical models. Sci Transl Med 2023;15:eabk1900.
55. Philip M, Schietinger A. CD8(+) T-cell differentiation and dysfunction in cancer. Nat Rev Immunol 2022;22:209–23.